

Citation for published version: Gonzalez-Solino, C, Bernalte, E, Metcalfe, B, Moschou, D & Di Lorenzo, M 2020, 'Power generation and autonomous glucose detection with an integrated array of abiotic fuel cells on a printed circuit board', Journal of Power Sources, vol. 472, 228530. https://doi.org/10.1016/j.jpowsour.2020.228530

10.1016/j.jpowsour.2020.228530

Publication date: 2020

Document Version Peer reviewed version

Link to publication

Publisher Rights CC BY-NC-ND

University of Bath

Alternative formats

If you require this document in an alternative format, please contact: openaccess@bath.ac.uk

General rights

Copyright and moral rights for the publications made accessible in the public portal are retained by the authors and/or other copyright owners and it is a condition of accessing publications that users recognise and abide by the legal requirements associated with these rights.

If you believe that this document breaches copyright please contact us providing details, and we will remove access to the work immediately and investigate your claim.

Download date: 09. Mar. 2023

Power generation and autonomous glucose detection with an integrated array of abiotic fuel cells on a printed circuit board

Carla Gonzalez-Solino^{1,2}, Elena Bernalte^{1,2}, Benjamin Metcalfe^{2,3}, Despina Moschou^{2,3}, Mirella Di Lorenzo^{1,2*}

¹Department of Chemical Engineering, University of Bath, Bath BA2 7AY, United Kingdom ²Centre for Biosensors, Bioelectronics and Biodevices (C3Bio), University of Bath, Bath BA2 7AY, United Kingdom

³Department of Electronic and Electrical Engineering, University of Bath, Bath BA2 7AY, United Kingdom

^{*}Corresponding author: m.di.lorenzo@bath.ac.uk

Abstract

Wearable technologies can enable effective management of life-threatening diseases. In such systems, miniaturisation leads to minimally invasive and lightweight devices that, whilst ensuring safety, allow patients to perform their everyday activities freely. By generating direct and continuous energy from physiological fluids at body temperature, glucose fuel cells (GFCs) provide an attractive and easy-to-miniaturise power source alternative to lithium batteries, which is. In this context, we explore for the first time the use of printed circuit boards (PCBs) for the development of integrated arrays of abiotic GFCs and successfully demonstrate their operation at physiological concentrations of glucose, both in a phosphate buffer and in synthetic interstitial fluid. Each GFC consists of a porous gold anode and a Pt/Au cathode in a single layer, and generates a maximum power of 14.3 µW cm⁻² in 6 mM of glucose, with a linear response to glucose within a concentration range that includes hypo- and hyperglycaemic values. We also demonstrate linear power output scale-up by electrically connecting in parallel four GFCs on PCB. Considering the simplicity of the system architecture and the ease of integration provided by PCBs, our pioneering work paves the way for exciting opportunities in the field of self-powered wearable diagnostics.

Keywords: Glucose fuel cell; Wearable technologies; Self-powered sensor; Lab-on-PCB; Power management system; Bioenergy harvesting

1. Introduction

Today's aging society poses increasing pressure on the development of effective technologies to support independent living of the elderly and patients with chronic diseases [1]. Such technologies can assist remote healthcare management in the patient's natural environment *via* seamless data collection over prolonged periods of time. Wearable healthcare devices hold promise as a way to improve patient care and chronic disease prevention and management while reducing costs, as the need for medical emergency consultations and hospital admissions are significantly reduced. To operate and transfer data, these systems require a power source, currently provided by standard lithium batteries [2]. An attractive alternative, which does not require charging or replacement and is easy-to-miniaturise for minimally invasive devices, is represented by Glucose Fuel Cells (GFCs) [3].

GFCs generate useful energy from any physiological fluid at body temperature. The chemical energy stored in the glucose naturally present in these fluids is directly converted into electricity by coupling the oxidation of glucose at the anode with the reduction of oxygen at the cathode [4]. Electricity generation by GFCs has been successfully demonstrated in mammals, thus proving the possibility to harvest energy from blood [5], serum [6] and saliva [7]. GFCs rely on the use of either metals or on enzymes as catalysts in order to function. Enzymes offer high specificity, but their low stability over time hampers their long-term use. Metal catalysts provide higher stability, however, their low specificity poses a problem for implantable and wearable applications, where both oxidant and fuel are present in the same electrolyte, leading to a mixed potential at both electrodes [8].

Despite recent improvements in terms of power output and stability, GFCs still generate a voltage that is too low (maximum 1 V) for most microelectronic devices, which require an input voltage between 1 and 3 V to operate [4]. A common strategy to overcome this limitation

and increase the power output is to electrically connect several fuel cell units, either in series or parallel. Recently, a GFCs stack in the series configuration was proposed to increase the voltage output in enzymatic fuel cells implanted in a lobster [9]. Such configuration, however, is impractical in real applications, due to short circuit currents and low internal resistance between the fuel cell units [9]. On the other hand, electrically stacking fuel cells in parallel increases the power generated, although DC-DC converters are usually required to boost the output voltage [10-12].

Practical wearable applications would, therefore, require the functional electrical integration of several fuel cells, along with the required electronics, in a compact and miniature device. An interesting platform to facilitate microelectronics integration for miniature GFC-based wearable devices is offered by Printed Circuit Boards (PCBs). PCB technology is characterised by established large-scale and, consequently, low-cost mass manufacturing [13]. PCBs have been proposed recently for the design and development of proton exchange membrane fuel cells [14, 15] and direct methanol fuel cells for small electronic applications [16]. Nevertheless, in GFCs applications, PCBs have only been used for housing DC-DC converters to boost the power output, with either paper-based [17] or textile-based [11] electrodes. As such, PCB technology has not yet been exploited for the development of a seamlessly integrated fuel cell microsystem. Moreover, no Lab-on-PCB microsystem capable of producing electrical power on-chip has so far been demonstrated.

In this context, for the first time we explore the use of commercially fabricated PCB-based gold-plated electrodes to build-up functional GFCs and demonstrate the suitability of PCB technology as a viable platform for integrated glucose/oxygen fuel cells stacks. The PCB electrodes are modified either with a highly porous gold structure or with platinum to generate respectively the anode and the cathode of the fuel cells. First, the electrochemical performance of both electrodes is thoroughly investigated. The resulting fuel cells are then tested both

individually and when electrically connected in a stack, in either phosphate buffer or synthetic interstitial fluid. The response of both individual GFCs and GFCs arranged in stacks to various concentrations of glucose, including hypo- and hyper- glycaemic physiological values, is also assessed for autonomous glucose detection applications.

2. Materials and methods

2.1 Materials

All chemicals were of analytical grade and used without further modification unless otherwise specified. All aqueous solutions were prepared with ultrapure water (18.2 M Ω cm⁻¹) from a Milli-Q system (Millipore, UK). Calcium chloride, HEPES sodium salt, hydrogen tetrachloroauric acid (HAuCl₄), potassium chloride, potassium ferricyanide, sodium phosphate dibasic (Na₂HPO₄) and sodium phosphate monobasic (NaH₂PO₄) were purchased from Alfa Aesar. α -D(+)-glucose was obtained from Fisher. Sulfuric acid, ammonium chloride, sodium chloride, sucrose, magnesium sulphate, lactic acid, ascorbic acid, uric acid, acetaminophen, and L-cysteine were purchased from Sigma Aldrich.

Unless otherwise specified, all the experiments were performed in air-equilibrated 0.1 M phosphate buffer pH 7.4 prepared from Na₂HPO₄ and NaH₂PO₄ dissolved in Milli-Q water. Stock solution of 2 M D(+)-glucose in phosphate buffer was kept overnight at room temperature prior to be used to allow mutarotation from α -monomer to β -monomer [18].

Synthetic Interstitial Fluid (SIF) was prepared by dissolving 2.5 mM CaCl₂, 10 mM HEPES sodium salt, 3.5 mM KCl, 0.7 mM MgSO₄, 123 mM NaCl, 1.5 mM NaH₂PO₄, 7.4 mM saccharose in phosphate buffer, as previously suggested [19]. The pH was adjusted to pH 7.4 by adding appropriate amount of 1 M HCl. The SIF was stored in dark and at room temperature when not used.

2.2 Characterisation of PCB-based gold-plated electrodes and fabrication of the GFC anode and cathode

The PCBs used in this work were adapted from a previous application [20]. Each PCB (42.5 mm length x 34.5 mm width) consisted of four rows that include a circular electrode (geometric area: 1.54 mm²) used as the anode, and a crescent electrode, used as the cathode (geometric area: 7.22 mm²), as shown in Figure 1. The surface morphology of the PCB gold-plated electrodes was analysed by scanning electron microscopy (SEM), using a JEOL JSM-6480LV coupled to an Energy Dispersive X-Ray Analysis (EDX) instrument. A conventional peripheral component interconnect (PCI), purchased from RS components (UK), was used to connect the PCB to an Autolab PG302N (Metrohm, UK) potentiostat. The latter was used to activate the PCB gold-plated electrodes prior to use, by cycling the potential from -0.5 V to 1.6 V during 12 cycles in 0.05 M H₂SO₄ and at a scan rate of 100 mV s⁻¹ in a three-electrode set-up, with Ag/AgCl as the reference electrode and platinum wire (diameter 0.5 mm, Alfa Aesar, UK) as the counter electrode. The same configuration was then used to electrochemically characterise the PCB gold-plated electrodes by cyclic voltammetry (CV) in 0.1 M KCl containing 5 mM potassium ferricyanide, at a scan rate varying from 5 to 200 mV s⁻¹.

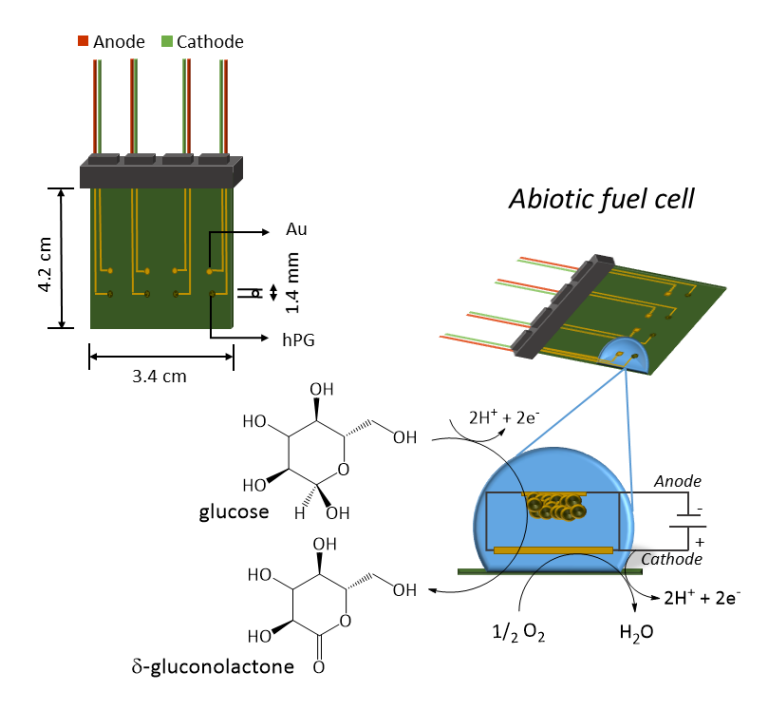


Figure 1. Schematic of the single layer fuel cell on a PCB used in this work, along with the reactions occurring at the anode and cathode. The anode is highly porous gold (hPG) deposited onto the PCB gold-plated electrodes (black dot in the schematic). The cathode is platinum sputtered onto the PCB gold-plated crescent electrodes (in silver colour in the schematic). Each PCB contained four pairs of anodes and cathodes, leading to an array of four fuel cells. During the operation, the electrodes were exposed to a droplet of the target solution.

For the fabrication of the GFC anode, a highly porous gold (hPG) structure was electrodeposited onto the PCB electrodes via the dynamic hydrogen bubbling template. In particular, the target electrodes were covered with a solution of 0.1 M HAuCl₄ and 1 M NH₄Cl. A current of -20 mA was then applied for 15 seconds, using Ag/AgCl as the reference electrode and platinum wire as the counter electrode, following the previous work by du Toit et al [21]. The electrodes were then washed with Milli-Q water, activated by cycling the potential in 0.05 M sulfuric acid for 2 cycles at 50 mV s⁻¹ scan rate and stored at room temperature until used.

The cathodes (Pt/Au) were obtained by sputtering a 50 nm film of platinum onto the PCB gold-plated crescent electrodes (HHV sputter coater, UK), under argon at a flow rate of 10 standard cubic centimetre minute, with a base and process pressure of 8.63×10^{-6} mbar and 4×10^{-3} mbar respectively, at a deposition rate of 1.1 Å s^{-1} .

The electroactive surface area of the PCB gold-plated and hPG-modified electrodes, was determined by CV tests as previously reported [22]. Briefly, the electrodes were immersed in 50 mM H₂SO₄ and the potential was cycled from -0.5 V to +1.6 V vs. Ag/AgCl at a scan rate of 50 mV s⁻¹. The electrochemical surface area (ESA, cm²) of the gold electrodes was then calculated using Equation 1:

$$ESA = \frac{Q}{386}$$
 Equation 1

Where Q is the charge of the electrode (μ C), and 386 μ C cm⁻² is the estimated charge for a 1 cm² polycrystalline Au electrode [22, 23]. Q was calculated by integrating the peak area of the gold oxide reduction (A V), divided by the scan rate of the cyclic voltammetry test (V s⁻¹). The roughness factor, RF, of the electrode was calculated as:

$$RF = \frac{ESA}{electrode\ geometric\ surface}$$
 Equation 2

The electrochemical activity of the hPG electrodes towards glucose was analysed by CV and chronoamperometry. CV tests were performed to determine the oxidation potential of glucose at the surface of the hPG electrodes, while chronoamperometry at different glucose concentrations was employed to assess the response of these electrodes to glucose. All electrochemical tests were performed in air-equilibrated 0.1 M phosphate buffer pH 7.4 containing 6 mM glucose unless otherwise specified. The chronoamperometric tests were performed at the optimal potential obtained from CV measurements. The sensitivity of the hPG

electrodes towards glucose was calculated from the slope of the calibration curve, b (μ A mM⁻¹), and referred to the geometric area (A, cm²) of the hPG electrode. The limit of detection (LOD) was calculated as 3 SD/b, where SD is the standard deviation of the blank.

The platinum electrodes (Pt/Au) were also characterised by linear sweep voltammetry (LSV) to study the catalytic reduction of oxygen. The tests were performed in a three-electrode setup with gold as the counter electrode and Ag/AgCl as the reference electrode, in 0.1 M phosphate buffer pH 7.4 containing 6 mM glucose, either saturated with O₂ or purged with N₂, to determine the onset potential and the current output for the reduction of oxygen, respectively.

2.3 Fuel cell set-up and characterisation

The hPG anode and the Pt/Au cathode were connected to a PicoData Logger ADC-24 (Pico Technology, PicoLog, UK), to monitor the potential difference between the two electrodes over time in air-equilibrated 0.1 M phosphate buffer pH 7.4 containing 6 mM glucose (Figure S1). The system was operated in open circuit potential (OCP) until reaching steady state. Afterwards, polarisation tests were performed by varying the external resistances applied to the system from $10~M\Omega$ to $1000~\Omega$ with a resistor box (RS components, UK) and by recording the resulting cell potential. The current generated by the fuel cell was calculated according to Ohm's law (V=I×R). Power curves were then obtained by using Equation 3.

$$P = E \times I$$
 Equation 3

Where: P is the power output (W); E is the cell voltage (V); and I is the current drawn from the fuel cell (A). The internal resistance (R_{int}) of the GFC was calculated from the linear fit of the ohmic region of each polarisation curve ($R_{int} = \Delta V/\Delta I$), as previously described [24].

The power output of the GFCs was scaled-up by generating stacks of fuel cells (up to four) electrically connected in parallel, as shown in Figure S2. The fuel cell response to glucose was

investigated by progressively varying the concentration of glucose in phosphate buffer, from $50 \mu M$ to 100 m M, while operating the fuel cell at the optimal external resistance.

The performance of the array of four GFCs connected in parallel (4-GFC) was also investigated in the presence of common interferences found in physiological fluids. The tests were performed by placing the PCB in a beaker containing 6 mM glucose in air-equilibrated 0.1 M PB pH 7.4 and the target interference. The power drop after each addition of interference was calculated as:

$$P_{drop} = \frac{P_0 - P_i}{P_0}$$
 Equation 4

Where: P_i is the power obtained after adding the interference (μW); and P_0 is the stable power output before adding the interference (μW).

2.4 Power management system

In order to demonstrate meaningful energy harvesting, the 4-GFC stack was connected to a commercial off-the-shelf power management system (BQ25504 EVM, Texas Instruments, TX), capable of operating from GFCs' low output voltage. The overall schematic diagram of the proposed energy harvesting system is shown in Figure S3. The BQ25504 system is designed to operate with input voltages as low as 100 mV, a range that covers most fuel cells. It has a built-in Maximum Power Point Tracking (MPPT) function that finds the OCP of the fuel cell and sets the operating point (by varying the effective load impedance seen by the fuel cell) to ~80% of this voltage. The OCP is sampled for 256 ms, which, for the GFCs proposed in this work, is sufficient for the cells to reach full OCP. The BQ25504 system also includes a battery management system, which was connected to a storage capacitor, as shown in Figure S3. Both the 4-GFC voltage and the voltage over the energy storage element were continually logged using a Pico datalogger to record the voltage over time.

3. Results and Discussion

3.1 Electrochemical and physicochemical characterisation of the printed circuit board electrodes

In this study, for the first time, commercially fabricated PCB-based gold-plated electrodes were used for the development of a GFC. First, the electrodes were electrochemically characterised. The results are shown in Figure S4. The *I-V* response of the PCB gold-plated electrodes is characterised by an oxidation peak at 1.4 V, (vs. Ag/AgCl), corresponding to the formation of gold oxide, and a reduction peak at a voltage of 0.9 V (vs. Ag/AgCl), corresponding to the reduction of the gold oxide (Figure S4a). This voltammogram is characteristic of electrochemically active and polycrystalline gold surfaces [23]. The ESA of these electrodes is 0.014 cm², with a roughness factor of 0.91. SEM and EDX analysis of their surface reveal a homogeneous and smooth morphology (Figure S5).

Further electrochemical characterisation of the electrodes was performed in 0.1 M KCl, containing 5 mM potassium ferricyanide (III) as a redox probe. At a scan rate of 50 mV s⁻¹, the peak to peak separation (Δ Ep) is 76 mV, which is slightly bigger than what expected for a Nernstian one-electron reaction [25]. As shown in Figure S4b and 4c, the peak current varied linearly with the square root of the scan rate (R^2 =0.99), typical of electrodes under diffusion-controlled mechanisms. Therefore, as expected for a gold-based electrode, the PCB gold-plated electrodes show a well-defined gold oxidation behaviour, making them a great basis for building the GFCs.

The PCB gold-plated circular electrode was then functionalised with highly porous gold (hPG) to generate the anode of the GFC. hPG is characterised by a honeycomb microstructure (Figure 2a), as previously observed [21, 26]. The *I-V* response in sulfuric acid shows a very stable and electrochemically active surface with the gold oxidation at ca. 1 V (vs. Ag/AgCl) and a peak,

corresponding to the reduction of gold oxide at ca. 0.9 V (vs. Ag/AgCl) (Figure S6a). Notably, two oxidation peaks at 1 V and 1.2 V vs. Ag/AgCl appeared in the Au-oxide region, which can be attributed to the crystallinity and structure of the hPG [27]. A similar behaviour has been previously reported for nano-porous gold [28, 29]. The ESA of the hPG electrode (Figure 2b) increased almost 127 times compared to the ESA of PCB gold-plated electrodes, with an effective area of 1.96 ± 0.15 cm².

In the presence of glucose, hPG generates two oxidation peaks (Figure S6b), as previously described [30]. To further characterise the catalytic oxidation of glucose by hPG, the reaction was investigated by chronoamperometry in a three-electrode set-up at an applied potential of 0.22 V vs. Ag/AgCl [31, 32]. A linear response up to 60 mM of glucose is observed (Figure 2c), with a sensitivity of 23 μ A mM⁻¹ cm⁻² towards glucose and a limit of detection of 40 μ M, which is in agreement with other porous gold electrodes previously reported [22, 33]. The low onset potential (-0.37 V vs. Ag/AgCl), along with a high sensitivity towards glucose, could be a result of the pore size and high specific surface area of hPG [18].

For fuel cell applications, where very negative onset potentials are sought for the anodic reaction, the low onset potential of the PCB hPG electrodes offers great advantage compared to other gold electrodes, characterised by glucose oxidation at more positive potentials [18, 34].

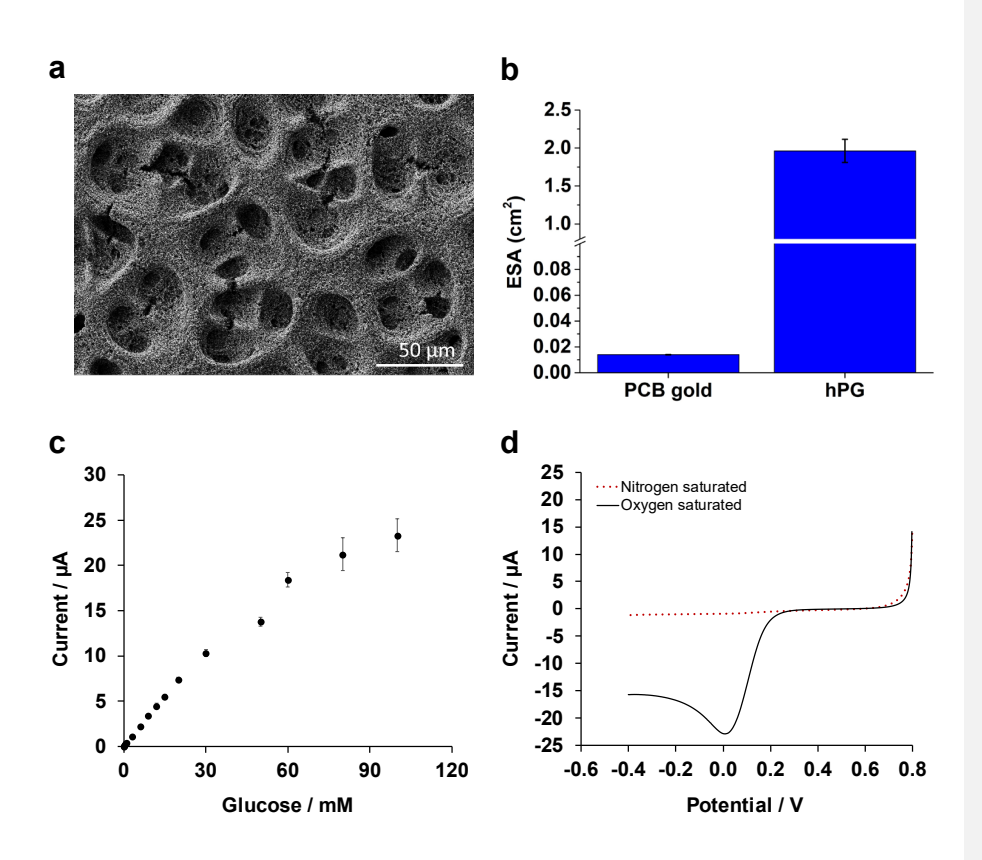


Figure 2. Characterisation of the PCB hPG electrodes. a) SEM image of the hPG electrode, taken with an acceleration voltage of 10.0 keV, a working distance of 6.0 mm and a magnification of 500X. b) Electrochemical surface area (ESA) of the hPG electrode, obtained from the reduction peak of the gold oxide in Figure S6a and using Equation 1. The error bars refer to the standard error of 10 replicates. c) Calibration curve obtained from the *I-t* response to glucose, concentration range: $50~\mu\text{M}$ - 100~mM (data from Figure S6c). Errors bars refer to the standard deviation of three independent electrodes. d) Investigation of the ORR at the cathode (PCB-based Pt/Au) by linear sweep voltammetry at a scan rate of 5~mV s⁻¹ in 0.1 M phosphate buffer pH 7.4, either saturated with N₂ (red line) or with O₂ (black line).

As shown in Figure 2d the oxygen reduction reaction (ORR) at the platinum surface of the PCB Pt/Au electrode in O₂-saturated phosphate buffer starts at $180\,\mathrm{mV}$ vs. Ag/AgCl, calculated with the two-tangent method. The ORR reaches a maximum current peak of $22.81\,\mu\text{A}$, at a potential

of 10 mV vs. Ag/AgCl. The ORR overpotential of the Pt/Au cathode is very similar to what observed with other catalysts, such as N-doped mesoporous carbon and Pt/C [35]. As expected, when tested in N₂-saturated phosphate buffer, no reduction current was observed. Moreover, the PCB Pt/Au electrode did not show any electrocatalytic activity towards 6 mM glucose within the potential window tested (Figure S6d), which is expected given the low specific surface area of the electrode. In this condition in fact, the oxygen reduction dominates the electrode potential, leading to faster reaction rates for the oxygen reduction compared to the glucose oxidation [36]. On the other hand, the high porosity of the hPG electrode favours the kinetically controlled oxidation of glucose, while oxygen is depleted across the porous structure [36]. Kerzenmacher's research group has reported similar conclusions using a porous Raney-type platinum electrode for the oxidation of glucose, with increased specific activity towards glucose when increasing the roughness of the Pt electrodes [6].

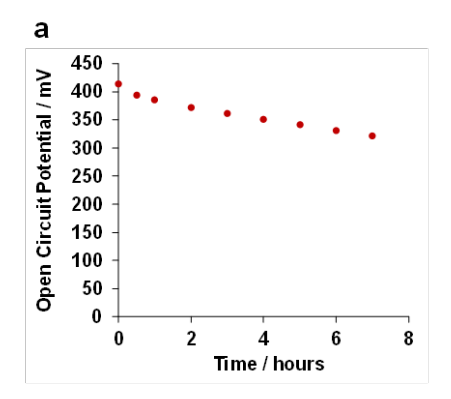
In conclusion, these results demonstrate that PCB hPG electrodes and smooth Pt/Au electrodes are suitable as anodes and cathodes for the oxidation of glucose and oxygen reduction in compartment-less abiotic fuel cells.

3.2 Characterisation of the glucose fuel cell

Once the PCB electrodes and the hPG anode and Pt/Au cathode were electrochemically characterised, the performance of the GFC in a single layer configuration was investigated. As discussed above, the single layer configuration is possible thanks to the high specific activity of hPG anode towards glucose, consequent to its high surface area and roughness [37, 38], along with the smooth surface of the Pt/Au cathode.

In the presence of 6 mM glucose in air-equilibrated phosphate buffer (0.1 M, pH 7.4), the GFC exhibited an OCP of 425 ± 30 mV. As a control, when PCB gold-plated electrodes (not functionalised with hPG) were coupled with the Pt/Au, no open circuit potential was observed for the same conditions of glucose and oxygen saturation (Figure S7). Nevertheless, such OCP is expected to fluctuate under different conditions of glucose and oxygen as the open circuit potential obeys the Nernst equation and is therefore dependent on the concentration of both fuel and oxidant [24].

After 1 hour of operation, the OCP of the GFC slowly decreases over time, as shown in Figure 3a. A similar voltage loss was reported by Katz et al. [39] and it was attributed to glucose depletion at the electrode surface over time. In the present study, however, the voltage is not recovered after adding fresh glucose solution to the fuel cell, which suggests that electrode inhibition or passivation is occurring on the surface of the hPG anode. Previous studies suggest that phosphate buffer anions might affect the oxidation of glucose [40]. In fact, when reactivating the hPG electrodes by CV (2 cycles) in 0.05 M sulfuric acid, the OCP was fully recovered.



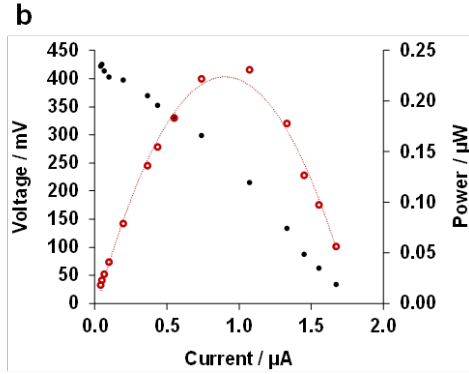


Figure 3. Electrochemical characterisation of the single GFC on PCB a) Stability of the open circuit potential over time in batch. b) Polarisation curve and power curve. Electrolyte: air-equilibrated 0.1 M phosphate buffer (pH 7.4) containing 6 mM glucose.

The polarisation test shows a steep drop in voltage as current is drawn from the system, until reaching a short circuit current of 1.68 μA (Figure 3b). This voltage drop could be attributed to a mixed effect of ohmic and mass transport limitations in our system. The fuel cell showed a lower internal resistance (180 k Ω) compared with fuel cells previously reported with a depletion design [41], which could be a result of the membrane-less design implemented in this study [36]. Still, the internal resistance of the GFC developed in this study is much higher than other abiotic GFCs reported in the literature based on selective catalysts such as Au/Pt [39] or Au nanowires [35] . The small geometrical area and length of our electrodes can contribute to the high internal resistance of our fuel cell [42]. In fact, the high internal resistance would explain the low power output of our fuel cell compared to other GFCs summarised in Table 1 [35, 39]. The maximum power output generated by the single fuel cell is $0.22 \pm 0.03~\mu W$ (n=3) at an operational voltage of 297 mV (Figure 3b). In terms of power density (referred to the geometric area of the anode), the proposed GFC has a power density peak of 14.3 μW cm⁻² in phosphate buffer.

Table 1. Comparison of several reported abiotic glucose fuel cells according to their design and power output.

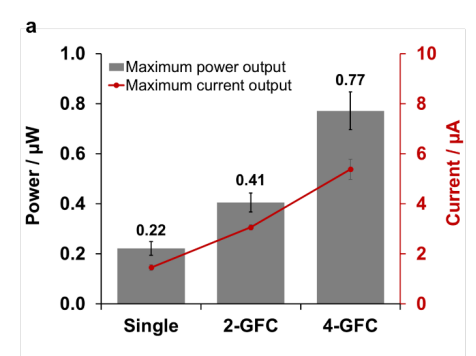
Anodic catalyst	Cathodic catalyst	Conditions	MPD μW cm ⁻²	Fuel cell design	Fabrication technology	Reference
hPG	50 nm Pt film	6 mM glucose 100 mM PB pH 7.4 RT 21% DO	14.3	single layer fuel cell	РСВ	this study
hPG	50 nm Pt film	6 mM glucose SIF pH 7.4 RT 21 % DO	1.6	single layer fuel cell	РСВ	this study
Raney Pt	mesh of SWCNTs	10 mM glucose 10 mM PBS pH 7.4 RT	3.4	depletion	CMOs	[41]
Raney Pt	Pt/Al	3 mM glucose PBS pH 7.4 37 °C 7% DO	2.9	single layer fuel cell	Silicon wafer	[43]
Raney- Pt/Ni	Raney- Pt/Al	5 mM glucose 10 mM PBS pH 7.4 37 °C 7% DO	2.0	single layer fuel cell	Silicon wafer	[44]
Porous Pt on ceramic substrate	Porous Pt	3 mM glucose PBS pH 7.4 7% DO	2.4	Depletion design	Silicon wafer	[45]
Pt/Ni	Sputtered Pt on porous support	5 mM glucose 10 mM PBS pH 7.4 37 °C 7% DO	2.0	stacked electrodes	Silicon wafer	[42]
Au/CB	Au ₆₀ /Pt ₄₀ on CB	5.4 mM glucose in human serum in-vitro	26	selective catalysts	Bucky-paper	[39]

AuNW	N-m-C	5 mM glucose 0.1 M PBS RT 21 % DO	64.3	selective catalysts	-	[35]
Al/Au/Zn O	Pt	5 mM glucose 0.1 M PB RT 21 % DO	16.2	selective catalysts	-	[46]
Pt/C/CP	Pt/C/CP	Anolyte: N ₂ - saturated 10 mM glucose in PB Catholyte: O ₂ - saturated PB 0.2 M PB pH 7.4 37 °C	20	H-cell	-	[47]

Legend: maximum power density (MPD), highly porous gold (hPG), phosphate buffer (PB), room temperature (RT), dissolved oxygen (DO), printed circuit board (PCB), single-walled carbon nanotubes (SWCNTs), synthetic interstitial fluid (SIF), complementary metal-oxide semiconductor (CMOS), phosphate buffer saline containing 150 mM NaCl (PBS), carbon black electrodes (CB), gold nanowires (AuNW), N-doped mesoporous carbon (N-*m*-C), carbon paper (CP).

3.3 Scaling-up the power output

Fuel cells stacking has been shown to be a powerful means to scale-up the power output. For practical wearable applications, however, the overall system should be minimally invasive. As such, a functional integration of all the electronic components, along with the fuel cells, is key. PCB technology offers the possibility to stack fuel cells effortlessly in either series or parallel arrangements within a single layer in a miniaturised chip. Parallel configuration is usually preferred over the series configuration for powering small electronic devices. Stacking in series usually suffers from short circuit currents [9], and has shown to be less efficient when the individual fuel cells do not perform equally [48]. Therefore, in this work we focused on the parallel connection only. We investigated two stack configurations on PCB: 2-GFC, consisting of two fuel cells; and 4-GFC, consisting of four fuel cells. The performance of both stacks was characterised in terms of power output and compared to the single fuel cell (Figure S8).



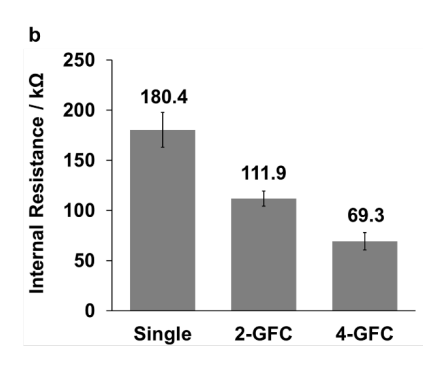


Figure 4. Comparison of performance of the two GFCs stacks with individual GFCs from polarisation tests in air equilibrated 0.1 M phosphate buffer pH 7.4 containing 6 mM glucose. a) Comparison of the power output. b) Comparison of the internal resistance. Data is the average of three independent replicates and the error bars refer to the standard error.

As expected, the OCP for both stacks coincides with the OCP for a single fuel cell, while the maximum current output increases linearly with number of fuel cells connected in parallel [49]. The highest current output for the single fuel cell was $1.6 \pm 0.1~\mu A$, while it increased up to $3.0 \pm 0.1~\mu A$ and $5.4 \pm 0.4~\mu A$ for the 2-GFC and 4-GFC respectively (Figure S8). The power output increased accordingly (Figure 4a). 2-GFC generated a total power output of $0.41 \pm 0.04~\mu W$, while 4-GFC generated a power output of $0.77 \pm 0.08~\mu W$, which is respectively 1.9 and 3.5 times higher than the power delivered by a single fuel cell. As observed in Figure 4b, the internal resistance decreased with the number of fuel cells connected in parallel, as previously reported [49].

A functional GFC based system needs not only to harvest energy but also to regulate it, to store it, and to deliver it effectively to the intended system load. This process is often neglected, yet the dynamics of the GFC can have a significant effect on the overall performance of the system [50]. Harvesting useful energy from GFCs is not trivial, this is primarily due to the low terminal voltages produced (often well below 1 V) but also because of the low power output. For any harvesting system, it is essential to operate the energy source in a manner that ensures

maximum power can be extracted. In order to achieve this, it is necessary to apply time varying load conditions using some method of MPPT [24]. Therefore, the 4-GFC stack was connected to the energy management system as shown in Figure S3. No external load resistor was used, and the storage element was a capacitor of 470 μ F. The stack showed a stable OCP of nearly 500 mV in air-equilibrated 0.1 M phosphate buffer containing 6 mM glucose. Figure 5 illustrates the effect of connecting 4-GFC to the energy management system. A large drop in the voltage is observed. This drop is caused by the MPPT system, characterised by a load that is periodically adjusted to maintain an ~20% reduction in the 4-GFC voltage relative to an OCP of nearly 500 mV. At the same time the boost-converter within the BQ25504, enables charging of the energy storage element, the voltage across the capacitor slowly rises to 2.6 V (a charge limit of 2.8 V was pre-determined by resistor settings within the BQ25504 EVM). This result demonstrates that 4-GFC is capable to power the energy harvesting system and that the harvested energy can be stored for future use. The time taken to charge the capacitor is directly related to both the capacitance and the power available at the output of 4-GFC.

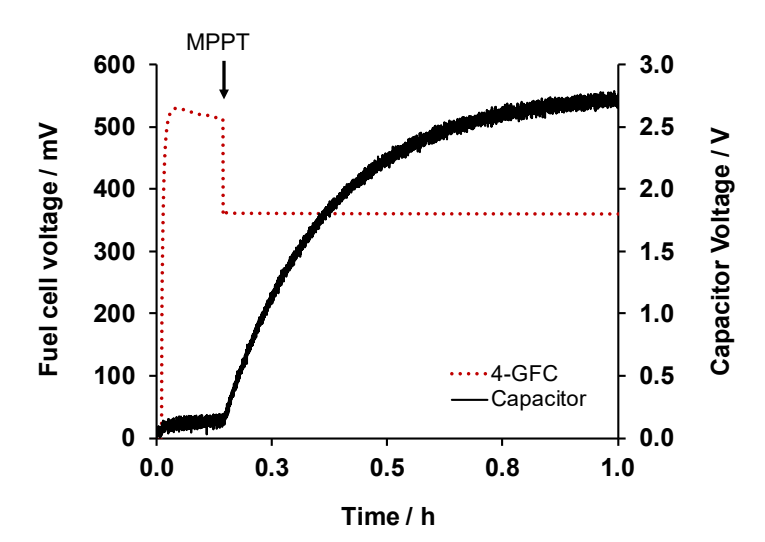


Figure 5. Capacitor being charged by the 4-GFC stack in air-equilibrated phosphate buffer 0.1 M pH 7.4 containing 6 mM glucose in batch. 4-GFC was connected to the

energy harvesting system, as shown in Figure S3, with no load resistor, and the storage element was a capacitor of 470 μ F. The arrow indicates the connection between the 4-GFC and the Maximum Power Point Tracking (MPPT). Experimental data corresponds to just one replicate.

3.5 Self-powered detection of glucose by the GFC

The power output generated by the GFCs is a consequence of the fuel (i.e. glucose) and oxygen concentration in solution [51]. Thus, GFCs can be exploited for the amperometric detection and quantification of glucose in physiological samples, leading to self-powered diagnostic applications. Moreover, the current response of the fuel cells, either individually connected or arranged in stacks, to physiological concentration of glucose, covering hyper-, hypo- and normoglycemic values, was therefore investigated (Figure 6). As shown, in each case a linear response within the range 300 µM - 9 mM was observed. The limited current obtained at high concentrations of glucose for all the GFCs tested could be attributed to fuel crossover between the anode and the cathode. This behaviour could be explained by the glucose oxidation at the Pt/Au electrode lowering down the OCP of the fuel cell, causing a simultaneous drop in power output at higher concentrations of glucose. Therefore, the Pt/Au electrode amperometric response to glucose was tested at increasing concentrations of glucose from 6 mM to 50 mM (Figure S9). The Pt/Au electrode showed a response to glucose that is more evident for glucose concentrations above 12 mM (Figure S9a), while it is negligible, compared to hPG, at lower concentrations (Figure S9b). This result is in agreement with the calibration curves obtained for the fuel cells that show no further power increase above 12 mM glucose. On the other hand, the linear response of GFCs obtained below 12 mM glucose is explained because Pt/Au electrode is not reactive towards glucose at this concentration range, therefore there is not such detrimental fuel crossover between cathode and anode. This is also supported by the results depicted in Figure S6d, where glucose did not interfere with the ORR at the Pt/Au electrode at

concentrations below 12 mM. The high specific surface area of the hPG electrode allows to develop the fuel cell at low concentrations of glucose. Nevertheless, the fuel cell should be optimised to operate at higher concentrations of glucose and to increase the linear range of the fuel cell for the self-powered detection of glucose.

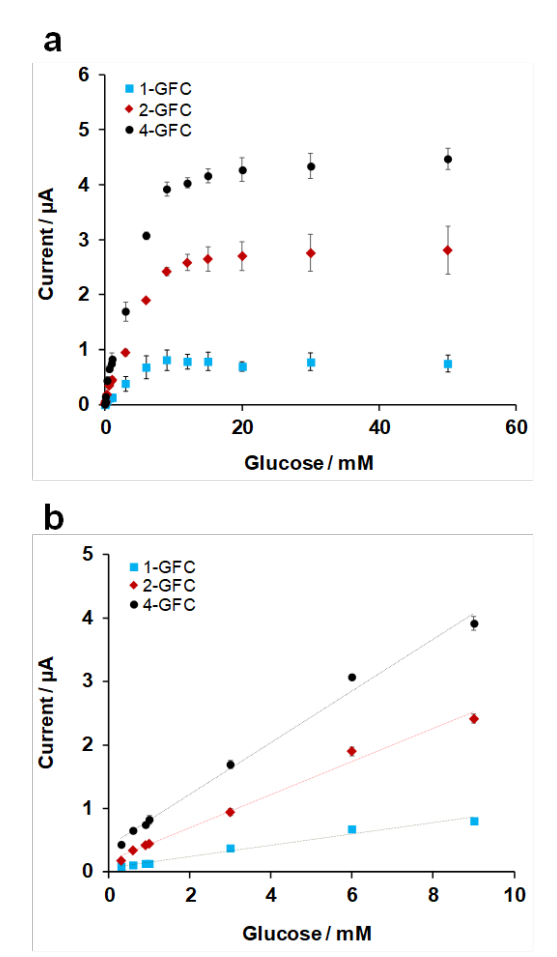


Figure 6. Current response to glucose in air-equilibrated 0.1 M phosphate buffer at pH 7.4: a) dynamic range of glucose tested from 50 μ M to 50 mM and b) linear range for the single GFC (R²=0.98), 2-GFC (R²=0.99) and 4-GFC (R²=0.99).

As shown, the GFCs allow the detection of hypoglycaemic (<3 mM pre-prandial glucose) and hyperglycaemic (>7 mM pre-prandial glucose) events [52]. Moreover, the sensitivity and limit of detection remained constant for each configuration tested. Specifically, the 4-GFC configuration showed a sensitivity of 8.8 μA mM⁻¹ cm⁻² and a limit of detection of 14 μM. 4-GFC could alert of abnormal glucose levels in interstitial fluid or blood; a current drop below 1.7 μA (Figure 6b) would indicate a hypoglycaemic event, while a current increase above 3.9 μA, would alert for hyperglycaemic conditions. It should be noted that these tests were performed under an air-saturated electrolyte, and therefore at a concentration of oxygen above the level in the physiological range (3.5% - 7%). According to the literature, lower concentrations of oxygen would lead to lower power outputs, and its effect should be investigated. Nevertheless, for the wearable application targeted in this study, the system can be designed so that the physiological fluid is exposed to air (for example by using air permeable coatings).

3.4 Performance in synthetic physiological fluids and effect of interferences

The performance of 4-GFC was further characterised in air-equilibrated synthetic interstitial fluid (SIF) containing 6 mM glucose. Figure S10 compares the polarisation and power curves of 4-GFC in both phosphate buffer and SIF. As shown, in SIF the maximum power output generated by 4-GFC decreased by a factor of 6 compared to the case of phosphate buffer. The polarisation curve in SIF is clearly governed by the ohmic losses; however, the internal resistance of 4-GFC is reduced, probably because of the larger conductivity of SIF (5.45 mS cm⁻²) compared to phosphate buffer (3.04 mS cm⁻²). The maximum current of 2.5 μ A delivered by 4-GFC at the lowest resistance tested (1000 Ω) is also 55 % lower than in phosphate buffer. These results suggest the possibility of inhibition mechanisms hampering the production of energy.

Commented [MDL1]: Add reference

Commented [MDL2]: Add reference

From the CV tests of the hPG electrode performed in a three-electrode set up, it was observed that in SIF the glucose oxidation shifted towards more positive potentials (Figure S11a). In particular, the oxidation starts at a potential of -271 mV, being 100 mV more positive than in phosphate buffer. In a similar way, the reduction of oxygen at the Pt/Au electrodes vs. Ag/AgCl shifted towards more negative potentials, with an onset potential of 158 mV and a maximum current output of $16.6~\mu A$ at a potential of -210 mV (Figure S11b).

The lower performance of 4-GFC in SIF is likely to be caused by the presence of Cl⁻ ions in solution, which have shown to inhibit the catalytic activity of metals even at trace level [18]. To demonstrate this, the performance of 4-GFC was tested in the presence of increasing concentrations of chloride ions. As shown in Figure 7a, the power density of the 4-GFC in 6 mM glucose decreased for increasing concentration of chloride ions. A concentration of 10 mM of NaCl, which is below typical chloride levels in physiological fluid, was already critical. Kim et al. [32] have suggested that the electrooxidation of glucose and resistance to chloride poisoning of gold electrodes depends on their nanostructure. Electrodes obtained with higher electrodeposition charges showed increased surfaces areas and greater tolerance to chloride poisoning. Little effect of chloride ions on the glucose oxidation reaction was in fact reported in a fuel cell based on gold nanowires [35], which suggests that the hPG morphology is more susceptible to chloride.

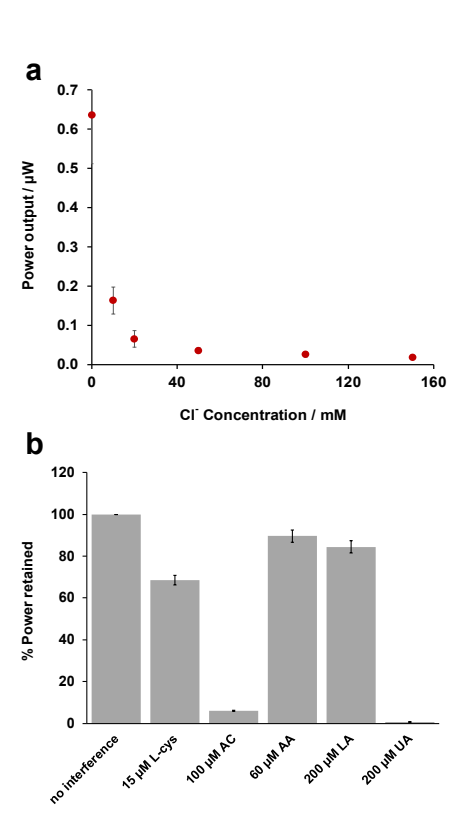


Figure 7. Interference effect on the power output generated by 4-GFC. a) Effect of chloride ions on the power output. b) Effect of common interferences present in SIF to the power output. The experiments were performed in air-equilibrated 0.1 M phosphate buffer containing 6 mM glucose at pH 7.4, with the fuel cell connected to the optimal external resistance, 69 k Ω . Error bars refer to the standard error (n=3). The interferences tested: L-cysteine (L-cys); acetaminophen (AC); ascorbic acid (AA); lactic acid (LA); and uric acid (UA) at normal physiological concentrations.

Chloride poisoning, therefore, poses a major hurdle in the use of hPG for wearable applications. The use of anionic membranes to filter out chloride ions would therefore be required in real applications. Superior resistance to chloride poisoning has been observed with alloys of gold with other metals, such as platinum, aluminium, or zinc oxide. These electrodes, however, usually suffer from higher overpotential for glucose oxidation and lower current densities [39, 46].

Although characterised by a lower complexity than blood, alternative physiological fluids contain molecules, such as amino acids and small metabolites, which can foul the electrode surface and interfere with the redox reactions [18, 53]. Micro and nano-porous gold structures have shown electro-catalytic activity towards several endogenous metabolites rather than glucose, such as uric acid, ascorbic acid or lactic acid, as well as to exogenous molecules such as acetaminophen [18]. The performance of 4-GFC was therefore analysed in the presence of interferences including ascorbic acid, lactic acid, uric acid, and acetaminophen at normal physiological concentrations (Figure 7b). Also, amino acids have shown a poisoning effect in metallic electrodes, such as platinum [18]. As such, the performance of 4-GFC was also tested in the presence of l-cysteine, used as an example of amino acid. As shown, ascorbic acid and lactic acid caused respectively only a 9 % a 14 % decrease in power output generated by 4-GFC. On the other hand, the presence of l-cysteine had a greater impact on the 4-GFC performance, with a 31.5 % drop in the power output. Nonetheless, the largest impact on the power output was caused by acetaminophen and uric acid had the largest, with a drop of 94.0 % and 99.4 %, respectively.

Similar studies in porous platinum electrodes demonstrated the different inhibitory effect of amino acids depending on their side chain, with basic and sulphur-containing amino acids having the strongest poisoning effect [54]. For micro- and nano-porous gold electrodes, however, there are no studies reported on the inhibitory effect of amino acids. Based on the results obtained in this work, future studies should, therefore, be considered in this direction.

4. Conclusions

Printed circuit boards open-up exciting perspectives on the development of integrated and minimally invasive power sources for cost-effective, up-scalable wearable healthcare technologies. In this work, for the first time we have demonstrated the use of PCB technology

for the design and development of an integrated array of single layer membrane-less glucose fuel cells, along with their functional arrangement in stacks for energy harvesting and glucose detection in physiological fluids, such as interstitial fluid. We characterised the performance of a single fuel cell and demonstrated power scaling up by electrically connecting in parallel four fuel cells in a single board. This stack showed an open circuit voltage of 425 mV and generated a total power output of 0.8 μ W at an operation voltage of 297 mV in the normal physiologic concentration of glucose. The 4-GFC array operated a power management system to charge a capacitor, thus demonstrating its capability to harvest useful energy. Subsequently, the self-powered detection of glucose by the GFCs array on PCB, within the linear range 300 μ M - 9 mM, was also demonstrated, with a sensitivity of 8.8 μ A mM⁻¹ cm⁻². The developed technology can, therefore, alert for abnormal glucose concentrations in a continuous and non-invasive manner. When tested in synthetic interstitial fluid, the power output was reduced to 0.1 μ W, probably due to the interference from chloride ions present in the fluid.

The PCB technology appears to be an excellent platform for stacking fuel cells in one single board for minimally invasive devices. This technology also offers the possibility of integrating fuel cells with active electronic components, such as DC-DC converters, pumps, valves or more complex microfluidic structures to operate *in vivo*. As such, this work pioneers an exciting branch of research into PCB-based miniaturised integrated technologies for autonomous wearable healthcare.

Acknowledgements

The authors would like to thank: the Engineering and Physical Sciences Research Council (EP/R022534/1) and the British Council/Newton Fund (UK-Turkey project 336872) for

funding; the University of Bath to support Carla Gonzalez-Solino's PhD scholarship; Dearbhla Mcbay and Sivapathasundaram Sivaraya for helping with the Pt deposition onto PCB electrodes; Philip Fletcher, from the Material and Chemical Characterisation facilities (MC²) at the University of Bath, for his help and assistance with the SEM and EDX characterisation; and David Chapman, from the Department of Electronic and Electrical Engineering at the University of Bath, for the electrical support during this project.

5. References

- [1] S. Malwade, S.S. Abdul, M. Uddin, A.A. Nursetyo, L. Fernandez-Luque, X. Zhu, L. Cilliers, C.-P. Wong, P. Bamidis, Y.-C. Li, Computer Methods and Programs in Biomedicine, 161 (2018) 233-237.
- [2] W. Liu, M.-S. Song, B. Kong, Y. Cui, Advanced Materials, 29 (2017) 1603436.
- [3] S. Cosnier, A. Le Goff, M. Holzinger, Electrochemistry Communications, 38 (2014) 19-23.
- [4] M. Gamella, A. Koushanpour, E. Katz, Bioelectrochemistry, 119 (2018) 33-42.
- [5] M. Cadet, S. Gounel, C. Stines-Chaumeil, X. Brilland, J. Rouhana, F. Louerat, N. Mano, Biosens. Bioelectron., 83 (2016) 60-67.
- [6] M. Frei, J. Erben, J. Martin, R. Zengerle, S. Kerzenmacher, J. Power Sources, 362 (2017) 168-173
- [7] P. Ó Conghaile, M. Falk, D. MacAodha, M.E. Yakovleva, C. Gonaus, C.K. Peterbauer, L. Gorton, S. Shleev, D. Leech, Analytical chemistry, 88 (2016) 2156-2163.
- [8] S. Kerzenmacher, J. Ducrée, R. Zengerle, F. von Stetten, Journal of Power Sources, 182 (2008) 1-17.
- [9] K. MacVittie, J. Halámek, L. Halámková, M. Southcott, W.D. Jemison, R. Lobel, E. Katz, Energy & Environmental Science, 6 (2013) 81-86.
- [10] C. Abreu, Y. Nedellec, A.J. Gross, O. Ondel, F. Buret, A.L. Goff, M. Holzinger, S. Cosnier, ACS Applied Materials & Interfaces, 9 (2017) 23836-23842.
- [11] W. Jia, X. Wang, S. Imani, A.J. Bandodkar, J. Ramírez, P.P. Mercier, J. Wang, Journal of Materials Chemistry A, 2 (2014) 18184-18189.
- [12] V. Oncescu, D. Erickson, Scientific Reports, 3 (2013) 1226.
- [13] D. Moschou, A. Tserepi, Lab on a Chip, 17 (2017) 1388-1405.
- [14] R. O'Hayre, D. Braithwaite, W. Hermann, S.-J. Lee, T. Fabian, S.-W. Cha, Y. Saito, F.B. Prinz, Journal of Power Sources, 124 (2003) 459-472.
- [15] O. Obeisun, C. Attingre, F.A. Daniels, J. Robinson, T. Mason, C. Gibbs, A.R. Kucernak, D.J. Brett, in: Meeting Abstracts, The Electrochemical Society, 2013, pp. 1373-1373.
- [16] A.P. Puerto, L. Hakola, A.R. Kucernak, in: Meeting Abstracts, The Electrochemical Society, 2018, pp. 1789-1789.
- [17] J.D. Yuen, A. Baingane, Q. Hasan, L.C. Shriver-Lake, S.A. Walper, D. Zabetakis, J.C. Breger, D.A. Stenger, G. Slaughter, Scientific reports, 9 (2019) 6931-6931.
- [18] K.E. Toghill, R.G. Compton, Int. J. Electrochem. Sci, 5 (2010) 1246-1301.

- [19] P. Bollella, S. Sharma, A.E.G. Cass, R. Antiochia, Electroanalysis, 31 (2019) 374-382.
- [20] P. Jolly, J. Rainbow, A. Regoutz, P. Estrela, D. Moschou, Biosensors and Bioelectronics, 123 (2019) 244-250.
- [21] H. du Toit, M. Di Lorenzo, Sensors and Actuators B: Chemical, 192 (2014) 725-729.
- [22] G. Sanzó, I. Taurino, R. Antiochia, L. Gorton, G. Favero, F. Mazzei, G. De Micheli, S. Carrara, Bioelectrochemistry, 112 (2016) 125-131.
- [23] L.D. Burke, P.F. Nugent, Gold Bulletin, 30 (1997) 43-53.
- [24] B.E. Logan, B. Hamelers, R. Rozendal, U. Schröder, J. Keller, S. Freguia, P. Aelterman, W. Verstraete, K. Rabaey, Environmental Science & Technology, 40 (2006) 5181-5192.
- [25] A.J. Bard, Electrochemical methods : fundamentals and applications, 2nd ed., John Wiley, New York Chichester, 2001.
- [26] S. Cherevko, C.-H. Chung, Electrochem. Commun., 13 (2011) 16-19.
- [27] C. Jeyabharathi, P. Ahrens, U. Hasse, F. Scholz, J. Solid State Electrochem., 20 (2016) 3025-3031.
- [28] H.S.C. Sáenz, L.P. Hernández-Saravia, J.S.G. Selva, A. Sukeri, P.J. Espinoza-Montero, M. Bertotti, Microchimica Acta, 185 (2018) 367.
- [29] M.D. Scanlon, U. Salaj-Kosla, S. Belochapkine, D. MacAodha, D. Leech, Y. Ding, E. Magner, Langmuir, 28 (2012) 2251-2261.
- [30] M. Pasta, F. La Mantia, Y. Cui, Electrochimica Acta, 55 (2010) 5561-5568.
- [31] L.Y. Chen, X.Y. Lang, T. Fujita, M.W. Chen, Scripta Mater., 65 (2011) 17-20.
- [32] B. Seo, J. Kim, Electroanalysis, 22 (2010) 939-945.
- [33] Y. Xia, W. Huang, J. Zheng, Z. Niu, Z. Li, Biosensors and Bioelectronics, 26 (2011) 3555-3561.
- [34] D.-W. Hwang, S. Lee, M. Seo, T.D. Chung, Anal. Chim. Acta, 1033 (2018) 1-34.
- [35] M. Chu, Y. Zhang, L. Yang, Y. Tan, W. Deng, M. Ma, X. Su, Q. Xie, S. Yao, Energy & Environmental Science, 6 (2013) 3600-3604.
- [36] Ó. Santiago, E. Navarro, M.A. Raso, T.J. Leo, Applied Energy, 179 (2016) 497-522.
- [37] Y. Li, Y.-Y. Song, C. Yang, X.-H. Xia, Electrochemistry Communications, 9 (2007) 981-988.
- [38] S. Park, T.D. Chung, H.C. Kim, Analytical Chemistry, 75 (2003) 3046-3049.
- [39] Y. Holade, K. MacVittie, T. Conlon, N. Guz, K. Servat, T.W. Napporn, K.B. Kokoh, E. Katz, Electroanalysis, 26 (2014) 2445-2457.
- [40] Y. Rong, R. Malpass-Evans, M. Carta, N.B. McKeown, G.A. Attard, F. Marken, Electroanalysis, 26 (2014) 904-909.
- [41] B.I. Rapoport, J.T. Kedzierski, R. Sarpeshkar, PLOS ONE, 7 (2012) e38436.
- [42] V. Oncescu, D. Erickson, Journal of Power Sources, 196 (2011) 9169-9175.
- [43] A. Kloke, B. Biller, U. Kräling, S. Kerzenmacher, R. Zengerle, F. von Stetten, Fuel Cells, 11 (2011) 316-326.
- [44] V. Oncescu, D. Erickson, Scientific Reports, 3 (2013) 1226.
- [45] M. Frei, J. Martin, S. Kindler, G. Cristiano, R. Zengerle, S. Kerzenmacher, J. Power Sources, 401 (2018) 403-414.
- [46] G. Slaughter, J. Sunday, Journal of Power Sources, 261 (2014) 332-336.
- [47] G.L. Caneppele, D.D. Reis, A.-M.B. Goncalves, G.C. Da Silva, C.A. Martins, Electroanalysis, 32 (2020) 1084-1092.
- [48] Y. Yang, T. Liu, K. Tao, H. Chang, Industrial & Engineering Chemistry Research, 57 (2018) 2746-2758.
- [49] R.A. Escalona-Villalpando, K. Hasan, R.D. Milton, A. Moreno-Zuria, L.G. Arriaga, S.D. Minteer, J. Ledesma-García, Journal of Power Sources, 414 (2019) 150-157.
- [50] M. Alaraj, J.-D. Park, Journal of Power Sources, 418 (2019) 225-232.
- [51] E. Katz, A.F. Bückmann, I. Willner, J. Am. Chem. Soc., 123 (2001) 10752-10753.

[52] World Health Organisation, in, 2016.
[53] G. Matzeu, L. Florea, D. Diamond, Sensors and Actuators B: Chemical, 211 (2015) 403-418.
[54] C. Köhler, M. Frei, R. Zengerle, S. Kerzenmacher, ChemElectroChem, 1 (2014) 1895-1900.